Title

Phasor Analysis of Fluorescence Lifetime Enables Quantitative Multiplexed Molecular Imaging of Three Probes

Journal

Analytical Chemistry, 94(41)

ISSN

0003-2700

Authors

Rahim, Maha K

Zhao, Jinghui

Patel, Hinesh V

et al.

Publication Date

2022-10-18

DOI

10.1021/acs.analchem.2c02149

Peer reviewed

HHS Public Access

Author manuscript

Anal Chem. Author manuscript; available in PMC 2023 November 27.

Published in final edited form as:

Anal Chem. 2022 October 18; 94(41): 14185–14194. doi:10.1021/acs.analchem.2c02149.

Phasor Analysis of Fluorescence Lifetime Enables Quantitative Multiplexed Molecular Imaging of Three Probes

Maha K. Rahim[#],
Department of Biomedical Engineering, University of California Irvine, Irvine, California 92697, United States

Jinghui Zhao[#],
Department of Biomedical Engineering, University of California Irvine, Irvine, California 92697, United States

Hinesh V. Patel,
Department of Biomedical Engineering, University of California Irvine, Irvine, California 92697, United States

Hauna A. Lagouros,
Department of Materials Science and Engineering, University of California Irvine, Irvine, California 92697, United States

Rajesh Kota,
Department of Biomedical Engineering, University of California Irvine, Irvine, California 92697, United States

Irma Fernandez,
Department of Biomedical Engineering, University of California Irvine, Irvine, California 92697, United States

Enrico Gratton,
Department of Biomedical Engineering, University of California Irvine, Irvine, California 92697, United States; Laboratory for Fluorescence Dynamics and Chao Family Comprehensive Cancer Center, University of California Irvine, Irvine, California 92697, United States

Jered B. Haun
Department of Biomedical Engineering, University of California Irvine, Irvine, California 92697, United States; Department of Materials Science and Engineering, Department of Chemical and Biomolecular Engineering, and Chao Family Comprehensive Cancer Center, University of California Irvine, Irvine, California 92697, United States

Corresponding Author: Jered B. Haun – Department of Biomedical Engineering, University of California Irvine, Irvine, California 92697, United States; Department of Materials Science and Engineering, Department of Chemical and Biomolecular Engineering, and Chao Family Comprehensive Cancer Center, University of California Irvine, Irvine, California 92697, United States; Phone: 949-824-1243; jered.haun@uci.edu.

[#]Author Contributions

M.K.R. and J.Z. contributed equally to the work. M.K.R., R.K., and J.B.H. devised the underlying concept for the work. M.K.R., R.K., and J.B.H. developed the detection panel. M.K.R., J.Z., H.K., and I.F. carried out the experimental work. M.K.R., J.Z., H.P., E.G., and J.B.H. carried out the data analysis. M.K.R., J.Z., and J.B.H. wrote the manuscript, which all authors reviewed and edited.

The authors declare no competing financial interest.

Abstract

The excited-state lifetime is an intrinsic property of fluorescent molecules that can be leveraged for multiplexed imaging. An advantage of fluorescence lifetime-based multiplexing is that signals from multiple probes can be gathered simultaneously, whereas traditional spectral fluorescence imaging typically requires multiple images at different excitation and emission wavelengths. Additionally, lifetime and spectra could both be utilized to expand the multiplexing capacity of fluorescence. However, resolving exogenous molecular probes based exclusively on the fluorescence lifetime has been limited by technical challenges in analyzing lifetime data. The phasor approach to lifetime analysis offers a simple, graphical solution that has increasingly been used to assess endogenous cellular autofluorescence to quantify metabolic factors. In this study, we employed the phasor analysis of FLIM to quantitatively resolve three exogenous, antibody-targeted fluorescent probes with similar spectral properties based on lifetime information alone. First, we demonstrated that three biomarkers that were spatially restricted to the cell membrane, cytosol, or nucleus could be accurately distinguished using FLIM and phasor analysis. Next, we successfully resolved and quantified three probes that were all targeted to cell surface biomarkers. Finally, we demonstrated that lifetime-based quantitation accuracy can be improved through intensity matching of various probe–biomarker combinations, which will expand the utility of this technique. Importantly, we reconstructed images for each individual probe, as well as an overlay of all three probes, from a single FLIM image. Our results demonstrate that FLIM and phasor analysis can be leveraged as a powerful tool for simultaneous detection of multiple biomarkers with high sensitivity and accuracy.

Graphical Abstract

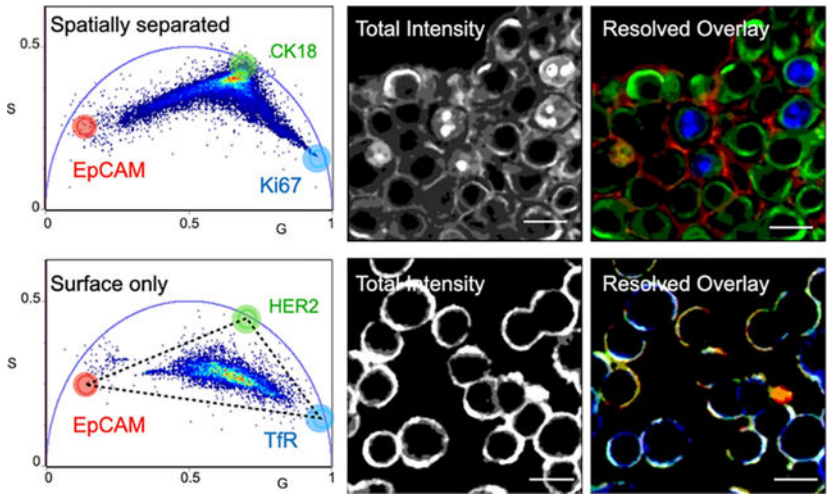

INTRODUCTION

Fluorescence microscopy is utilized extensively across biological sciences to visualize cells and tissues in exquisite detail. This is achieved by tagging molecules of interest with exogenous fluorescent dyes, proteins, and/or nanocrystals.[1] In some cases, endogenous biomolecules can exhibit their own native fluorescence signal, termed autofluorescence, which has generally been linked to cellular metabolism, energy production, and/or stress.[2–7]

Multiple targets are commonly visualized within the same sample using fluorescent probes that exhibit distinct spectral properties and a microscope with appropriate optical filters. In this manner, each probe is imaged separately, and the individual images are overlaid to compare spatial localization and relative intensity for each fluorescent probe. While traditional fluorescence microscopy is generally effective for correlative studies, quantifying signals can be challenging due to variations in illumination and detection efficiencies across different spectral windows, particularly when spanning large differences in wavelength. Moreover, time is required to change filters and acquire separate images, which can hinder live cell imaging and tracking studies. Finally, multiplexing capacity is often limited to around four different fluorophores to minimize the spectral overlap and ease data analysis, and adding more spectral channels is challenging due to limited spectral bandwidth.[8,9]

The fluorescence lifetime is the duration of fluorescence emission following excitation. This fundamental property provides an alternative means to distinguish fluorescent probes that are orthogonal to spectral properties. A general advantage of using lifetime is that a single image could be used to simultaneously assess multiple molecular targets, which would aid colocalization and live cell tracking studies. Fluorescence lifetime imaging microscopy (FLIM) is a technique that measures lifetime decays on a pixel-by-pixel basis using a confocal laser scanning format.[10] FLIM has successfully been used to detect lifetime changes for endogenous fluorescent species such as the metabolic cofactors NAD(P)H and FAD, which have been correlated with cell metabolism, phenotype, and age, as well as drug distribution and disease states such as cancer, Alzheimer's, and Parkinson's.[5,7,11–21] Application of FLIM is also growing rapidly for Forster resonance energy transfer (FRET) studies, whereby the donor lifetime serves as an absolute reference for the FRET signal, allowing results to be internally calibrated across different experiments.[22–25] However, FLIM has predominantly been limited to applications employing a single fluorescent molecular imaging probe that displays different context-dependent lifetimes or up to two different fluorescent molecular imaging probes within the same spectral window.[26–33]

A major factor that has impeded the multiplexing potential of FLIM has been the technical challenge of representing and analyzing lifetime data, which comprises an emission decay that can vary over time in both function and magnitude. For a single fluorescent species, the emission decay can readily be fit to an appropriate function, typically a single exponential, and lifetime magnitude can be characterized as the half-life. However, this curve fitting approach becomes exceedingly complex for probe mixtures and thus has been limited to at most one fluorescence species with variable lifetime or two different fluorescence species.[26,32,34–36] Many studies have taken a simpler time gating approach, in which emission is collected during excitation and after a set time delay. But time gating is typically limited to very long lifetimes and probes must be resolved using calibrations or phenomenological relationships.[26,37–39] Alternatively, the combinatorial use of both spectral and temporal signatures has been used to provide additional information for unmixing,[40] but this ultimately limits multiplexing potential. The phasor approach to fluorescence lifetime analysis was developed to circumvent the need to fit or time gate and is fully independent of spectral properties.[41] This powerful method transforms lifetime decays into frequency space at each pixel of a FLIM image, and the results are represented on a polar scatter plot that is called the phasor diagram. Different lifetime decay magnitudes and functions

appear at unique locations on the phasor diagram based on their modulation and phase shift, which enables simple, graphical comparisons.[5,42] Pixels containing only a single fluorescent species appear at the intrinsic phasor location for that species. Alternatively, pixels containing mixtures of fluorescent species with different intrinsic phasor locations are distributed between those locations in a manner that correlates to the relative amount of each species present. The linear property of the phasor approach makes it possible to employ simple vector math to determine the relative contributions of each fluorescent species to the total intensity within each pixel.[43] To date, FLIM and phasor analysis have been used to resolve relative contributions of three endogenous fluorescent species within cellular autofluorescence[5,7,11–18,21] or between autofluorescence and administered drugs.[19,20] Extension of these methods to cells that have been labeled with as many as three exogenous fluorescent probes has also been demonstrated, but these works were limited to general stains that also had different spectral properties.[44,45] To date, validation of FLIM/phasor analysis using exogenous fluorescent probes with the same spectral properties in a context relevant to molecular imaging has been lacking. This is critically important because, if successful, it would significantly increase the overall detection capacity of traditional fluorescence microscopy,[8,9] which could also be applied to more advanced multiplexing methods such as hyperspectral imaging,[46,47] combinatorial spectral/lifetime encoding,[48] and iterative staining strategies.[49–51]

In this work, we demonstrate that FLIM and phasor analysis can be used to simultaneously detect three molecular imaging probes using only fluorescence lifetime information. We utilized two organic dyes with distinct lifetimes, Alexa Fluor 555 and Bodipy TMR, as well as a long-lifetime quantum dot. First, we show that intrinsic phasor locations for each molecular probe remain consistent and reproducible after bioconjugation to antibodies and targeting to cells. Next, we use the probes to label molecular targets located in different regions of a cell, specifically the surface via epithelial cell adhesion molecule (EpCAM), cytoplasm via cytokeratin 18 (CK18), and nucleus via Ki67. This panel is used to confirm that phasor analysis can resolve different lifetimes and reconstruct single-probe images with high fidelity. We then detect three spatially colocalized biomarkers and attain qualitatively similar results. However, we also observe that quantitative accuracy can depend on the fractional intensity of the molecular probes present, specifically when brighter probes overwhelm signals from dimmer probes. To address this issue, we introduce an intensity matching concept by which the signal from brighter probes is purposefully and controllably titrated down by addition of an unlabeled antibody. After intensity matching, phasor analysis accurately reproduces the relative contribution and quantitative signal intensity for all probes. This work will significantly enhance the fluorescence imaging toolbox by enabling colocalization studies with only a single excitation scan and by increasing total multiplexing capacity via the addition of orthogonal lifetime information.

RESULTS AND DISCUSSION

Fluorescence Lifetime Probes.

Fluorescent species including Alexa Fluor 555 (AF555) and Bodipy TMR dyes, as well as a cadmium selenide/zinc sulfide quantum dot with 585 nm emission (Qdot 585), were

selected as the lifetime probe panel. Emission signals were similar for each species, centered at 575–580 nm (Figure 1A). However, fluorescence lifetimes were clearly distinct, mapping to unique locations on the phasor plot (Figure 1B). Lifetime data were obtained using FLIM with a white light laser and the same spectral filters (excitation: 534 ± 20 nm, emission: 560–660 nm). Thus, this fluorescence lifetime probe panel is ideally suited to simultaneous imaging and subsequent resolution of different biomarkers on a pixel-by-pixel basis using the phasor diagram.

Resolving Biomarkers That are Spatially Restricted.

We first set out to resolve the three lifetime probes after intentionally distributing them to different locations on a cell. This strategy simplifies analysis, since the majority of pixels within a FLIM image contain only a single probe, while the minority of pixels contain at most 2 probes. We localized each probe to a different cellular compartment using monoclonal antibodies. Specifically, we targeted Qdot 585 to the plasma membrane surface via the epithelial cell adhesion molecule (EpCAM), Bodipy TMR to the cytoplasm via cytokeratin 18 (CK18), and AF555 to the nucleus via Ki67. MCF7 breast cancer cells were selected for this study because they are known to be positive for all three biomarkers. However, initial tests demonstrated that the intensity of αCK18-Bodipy TMR was substantially higher than those of other biomarker–probe combinations, likely due to an elevated endogenous CK18 expression level. This would pose a significant challenge for lifetime-based probe detection, since the αCK18-Bodipy TMR signal would dominate the other biomarker-probes, potentially masking signals. To mitigate this effect, we reduced αCK18-Bodipy TMR intensity by mixing with the unlabeled αCK18 antibody at various ratios and found that 10:90 (labeled/unlabeled) was optimal (see Figure S1 in the Supporting Information). Importantly, signal intensity scaled linearly with the labeled/unlabeled antibody ratio, enabling straightforward calibration back to the expected intensity value of the undiluted sample.

Phasor plots and intensity images for MCF7 cells after labeling with each individual biomarker-probe combination (CK18 at 10:90 dilution, others no dilution) are shown in Figure 2A–C. The phasor locations closely matched those determined in solution (Figure 1B), although a slight shift toward the center of the phasor was noticeable for each probe. This shift can be attributed to a small contribution from cellular autofluorescence, which was minor and remained consistent across all images. Additionally, corresponding intensity images confirmed that the fluorescence signal emanated from within the intended cellular compartment. Next, all three biomarker probes were used in combination (Figure 2D). The resulting phasor diagram includes pixels containing only one molecular probe, predominantly αCK18-Bodipy TMR, as well as pixels that contained a combination of αEpCAM-Qdot 585 and αCK18-Bodipy TMR or αCK18-Bodipy TMR and αKi67-AF555. Notably, combinations of αEpCAM-Qdot 585 and αKi67-AF555 were absent, since these biomarkers are spatially restricted. Using custom software (SimFCS), we applied a color gradient to the phasor diagram to convey relative contribution to intensity for each probe and painted a corresponding image with this color map (Figure 2E), which clearly demarcated the different cellular compartments. Finally, we fully resolved each fluorescent species using phasor analysis and generated intensity images for each individual biomarker-probe target

(Figure 2F(i–iii)), which qualitatively matched the single-probe images (Figure 2A–C). A pseudocolored overlay image showing the overlap of each biomarker probe is shown in Figure 2F(iv). We contend that the combination of the overlay image (Figure 2F(iv)) and the direct interaction map on the phasor diagram (Figure 2D(i)) combine to provide the best and most complete information about spatial colocalization.

We also evaluated SK-BR-3 cells, which are positive for EpCAM and CK18 but have low Ki67 expression. Signal modulation was again needed for CK18 through dilution with the unlabeled antibody (see Figure S2 in the Supporting Information). The results can be found in Figure S3A–C in the Supporting Information and confirmed specific labeling and intrinsic phasor locations observed for MCF7 cells. Phasor diagrams were dominated by pixels containing the combination of αEpCAM-Qdot 585 and αCK18-Bodipy TMR due to low Ki67 expression. Importantly, expression patterns were accurately recapitulated across painted gradient images, resolved single-probe images, and the pseudocolored overlay. The findings for both MCF7 and SK-BR-3 cells confirmed that three probes can be resolved with high fidelity using only the phasor analysis of the fluorescence lifetime from a single FLIM image. We reiterate that reduction of the αCK18-Bodipy TMR signal was required in both cases to achieve these results. Without dilution, pixels that did not contain αCK18-Bodipy TMR may not have been detectable under the relatively low laser power that would have been required to prevent detector saturation. This could have been addressed by capturing images at different laser powers, but this would take more time and present calibration challenges. More importantly, αCK18-Bodipy TMR may have dominated the other biomarker probes present within the same pixel, which would have affected lifetime-based resolution accuracy and could not have been addressed by capturing multiple images.

Detecting Biomarkers That are Spatially Colocalized.

Next, we advanced to three biomarkers that can be present within the same pixels. The Qdot 585, Bodipy TMR, and AF555 lifetime probes were conjugated to antibodies targeting the surface biomarkers EpCAM, HER2, and transferrin receptor (TfR), respectively. Different breast cancer cell lines (SK-BR-3, MCF7, MDA-MB-231, MCF10A) were used to modulate the biomarker expression level. Single-probe stains for each cell line confirmed that intrinsic lifetimes and staining patterns remained consistent in all contexts (see Figure S4 in the Supporting Information). We then stained each cell line with all three probes simultaneously, which resulted in distinct phasor patterns for each cell line due to varying biomarker expressions (Figure 3A–D(i)). Phasor diagrams for SK-BR-3 cells were dominated by HER2 and TfR, with only minor contribution from EpCAM. As expected, phasor diagrams for the HER2 low cell lines MCF7, MDA-MB-231, and MCF10A contained pixels predominantly located between αTfR-AF555 and αEpCAM-Qdot 585, with minimal αHER2-Bodipy TMR contribution. Representative images showing total intensity, resolved intensity for each probe, and pseudocolored overlays (Figure 3A–D(ii–vi)) illustrate the utility of this approach to distinguish the contribution of each fluorescent probe to the total intensity on a pixel-by-pixel basis for three colocalized biomarkers.

The relative fraction of each biomarker probe was also determined across numerous triple stain images (Figure 3A–D(vii)), and this information was used to quantify mean intensity

(Figure 3E). We then compared mean intensities for each resolved probe to mean intensities obtained from singlestain images (see Figure S4 in the Supporting Information) and found statistically significant differences for EpCAM (all but MCF7) and HER2 (all but SK-BR-3). No statistical differences between resolved triple stain and single-stain results were found for TfR, indicating that the phasor analysis of the lifetime was fully quantitative in that case. These findings were directly illustrated by normalizing the resolved triple stain results by the corresponding single stain (Figure 3F). We observed that the lifetime-based resolution underreported signal for EpCAM and HER2 in some cases, with decreases that were as much as 40% for EpCAM (SK-BR-3) and 75% for HER2 (MCF7). We note that these cases were all characterized by very low fractional intensity (<10%) relative to one or both of the other biomarker probes. Relative signal disparities can result from differences in endogenous expression, the brightness of the probe, or both. Brighter probes and/or higher expression biomarkers dominated the total lifetime signal, leading to phasor analysis errors for dimmer probes and/or lower expression biomarkers. For EpCAM, which is highly expressed by SK-BR-3 cells,[52–54] the low signal was related to suboptimal excitation of Qdot 585 so as to enable simultaneous imaging with the dyes. For HER2, the low signal was entirely related to expression. Based on these results, we postulate that the accuracy of lifetime resolution using phasor analysis may be dependent on the fractional intensity of the molecular probes.

Improving Signal Fidelity and Quantitation through Intensity Matching.

To develop a robust method for quantitative lifetime resolution, we extended our intensity matching strategy initially employed for spatially separated biomarkers to colocalized biomarkers using SK-BR-3 cells. Unmodified anti-HER2 and anti-TfR antibodies were mixed at different ratios (100:0, 50:50, 30:70, and 10:90) with αHER2-Bodipy TMR and αTfR-AF555, respectively. In both cases, intensity decreased proportionally with the relative amount of the unmodified antibody, producing linear correlations (see Figure S5 in the Supporting Information). Based on these results, we performed multiplexed imaging studies with SK-BR-3 cells in which HER2 and TfR were both stained with dyelabeled/unlabeled antibody ratios of 30:70 or 10:90, while αEpCAM-Qdot 585 was left undiluted (100:0). As expected, phasor patterns spread progressively toward the αEpCAM-Qdot 585 vertex (red circle) as αHER2-Bodipy TMR and αTfR-AF555 were diluted (Figure 4A,B compared to Figure 3A(i) for undiluted case), corroborating that αEpCAM-Qdot 585 increased in fractional contribution. Total intensity for the FLIM images decreased with dilution, as did the resolved HER2 and TfR images, but EpCAM became increasingly distinguishable (compared to Figure 3A(ii–v)). The mean intensity was calculated for a series of images, and signal intensities for HER2 and TfR were converted to the signal that would be expected without dilution using respective calibrations (Figure 4C). There were no statistically significant differences between the mean intensity from single stains and the resolved triple stains for both HER2 and TfR under any of the dilution conditions ($p >$ 0.05 for all cases). For EpCAM, dilution of αHer2-Bodipy TMR and αTFR-AF555 by 30% improved phasor analysis resolution and resulted in no statistically significant difference relative to the single-stain counterpart. Adjusted mean intensities were again normalized by nondiluted single-stain intensities (Figure 4D), which further confirmed that intensity matching improved signal fidelity for EpCAM to >85% for the 30% dilution condition. Interestingly, further dilution of αHer2-Bodipy TMR and αTFR-AF555 to 10% lowered

accuracy for EpCAM, resulting in a statistically significant difference to the single stain. Although the fractional contribution of EpCAM was higher for this case, signal recovery was likely affected by lower overall intensity, possibly due to the influence of cellular background and/or calibration errors. Thus, it appears that elevating fractional contribution up to ~10% using the dilution strategy is advantageous, but further changes are not needed and can even be detrimental. Returning to the 30% dilution case, we do note that HER2 and TfR accuracies both decreased slightly. Hence, it may be advisable to perform imaging under both nondiluted and intensity-matched conditions in parallel samples to ensure that all probes are quantitatively resolved with the highest accuracy.

Validation of Intensity Matching Approach.

Finally, we implemented the intensity matching strategy for MCF7, MDA-MB-231, and MCF10A cell lines. Since each has low EpCAM and HER2 expression, dilution was only required for TfR-AF555. Fluorescence intensity again decreased proportionally to the amount of the unmodified anti-TfR antibody (see Figure S6 in the Supporting Information), and we chose to employ a 30% dilution. Phasor diagrams from multiplexed images are shown in Figure 5A–C(i) and clearly shifted toward the αEpCAM-Qdot 585 vertex (red circle) due to increased fractional contribution (compared to Figure 3B–D(i)). Although less noticeable, broadening of the phasor signature toward the αHER2-Bodipy TMR vertex (green circle) was also observed. Fractional contributions (Figure 5A–C(iv)) for EpCAM and HER2 also increased to 10% or greater. Importantly, quantitative resolution of EpCAM and HER2 expression both improved using intensity matching, with no statistically significant differences to single stains (Figure 5D), and fidelity was at ~90% (Figure 5E). The only exception was HER2 for MDA-MB-231 cells, for which fidelity was only 68%. This was likely caused by very low HER2 expression, acting in combination with a low total signal that was likely to be at or near the level of autofluorescence. As a result, small errors in the phasor analysis may have accumulated into underreporting of HER2. We note that signal recovery accuracy was worse when TfR-AF555 was diluted to 10% (see Figure S7 in the Supporting Information). As observed with SK-BR-3 cells, TfR signal reporting accuracy from the triple stain decreased to ~80% for MDA-MB-231 and MCF10A cells with dilution. This may have been due in part to the calibrations that were used to adjust back to the expected signal without dilution, which could be resolved using more advanced correction factors. However, this finding likely confirms that both normal and intensity-matched measurements may need to be made to ensure accurate quantification. To help illustrate this point, we have summarized the optimal labeling conditions and results for each biomarker probe and cell line in Table 1. Moving the FLIM/phasor multiplexing method forward into practice will require refinement of intensity matching concepts, particularly for samples in which expression is unknown, such as tumor tissues. A basic guideline would be to match probe brightness such that expressions of all biomarkers are benchmarked relative to each other. This is effectively what was done for EpCAM with SK-BR-3 cells to compensate for the low QD signal in Figure 4. Another strategy would be to intentionally allow for one or more probes to be brighter than the others, presumably because the expression of the corresponding biomarkers is low but still biologically relevant. This is effectively what was done for HER2 with MCF7, MDA-MB-231, and MCF10A cells in Figure 5. A fully agnostic approach would be to perform a systematic dilution of

all probe–biomarker combinations in parallel using separate samples, although this would require substantial effort. Alternatively, it might be possible to modulate the signal for one or more probes after imaging using competitive binding or partial probe release using a strategy, similar to those employed for iterative staining methods.[49–51]

CONCLUSIONS

We have demonstrated that lifetime-based imaging using FLIM and phasor analysis can discriminate three exogenous molecular probes, resulting in simultaneous resolution of different biomarkers either within or on the surface of cells. Moreover, we showed that the phasor unmixing algorithm is accurate for strong signals emanating from higher expression biomarkers and/or brighter probes. We also found that accuracy for lower expression biomarkers and/or dimmer probes can generally be enhanced by matching signal intensities between the different probe–biomarker combinations employed. This work will help expand the multiplexing capacity for fluorescence imaging, since lifetime panels can be developed for each spectral window, as well as possibly being incorporated into iterative staining workflows. Furthermore, the phasor diagram intrinsically displays an interaction map for different biomarkers, making colocalization studies straightforward and inherently quantitative, since only a single excitation scan was required. In future work, we will seek to further expand lifetime multiplexing to four, five, and even higher-order probe numbers. This would include additional organic dyes and possibly different types of quantum dots. Higher-order multiplexing potential already resides within the phasor analysis algorithm capabilities, at least theoretically,[43,44] if second and third harmonics can be leveraged. Thus, the primary limitation will be identifying compatible probe panels with lifetimes that are sufficiently distinct to meet the needs of a given cell labeling and imaging application.

MATERIALS AND METHODS

Materials.

Breast cancer cell lines MCF7, SK-BR-3, and MDA-MB-231, as well as breast epithelial cell line MCF10A, were obtained from ATCC (Manassas, VA). Cell culture reagents were purchased from Corning (NY) unless otherwise noted. TCO-NHS ester and Tetrazine-NHS ester were purchased from Click Chemistry Tools (Scottsdale, AZ). Qdot 585 amino (PEG), AF555-NHS ester, and Bodipy TMR-NHS ester were purchased from Thermo Fisher (Waltham, MA). Primary antibodies anti-EpCAM (CD326, Mouse IgG2b, clone 9C4), anti-cytokeratin 18 (CK18, Mouse IgG1, clone DA-7) were purchased from BioLegend (San Diego, CA). Anti-TfR (transferrin R, Mouse IgG1, clone # 29806) was purchased from the R&D System (Minneapolis, MN). Anti-HER2 (Herceptin) was a gift from Dr. Edward Nelson at UC Irvine Medical Center.

Preparation of Tetrazine-Modified Quantum Dots.

Amine-terminated Quantum dot 585 (Qdot 585) was modified with amine-reactive tetrazine-NHS, as we have reported.[55–57] Briefly, 75 μL of Qdot 585 (8 μM stock concentration) was reacted with 50 equiv of tetrazine-NHS in PBS solution containing 10% DMF and 10% sodium bicarbonate at room temperature for 3 h. The reaction product was purified using

an Ultra-4 centrifugal filter with a 10,000 molecular weight cutoff (Millipore Sigma), with three successive rounds of concentration and dilution with PBS. The absorption of modified Qdot 585 was recorded at 570 nm wavelength, and the concentration of the product was calculated by fitting it in a standard curve using a NanoDrop (Thermo Fisher).

Antibody Modification.

Anti-EpCAM antibody was modified with 30 molar excess of (*E*)-cyclooct-4-enyl-2,5-dioxopyrrolidin-1-yl carbonate (TCO-NHS Ester, Click Chemistry Tools). Anti-HER2 and anti-CK18 were reacted with 5 and 10 equiv of Bodipy TMR-NHS, respectively. AntiTfR and anti-Ki67 were modified with 5 and 30 molar equiv of AF555-NHS, respectively. Briefly, antibodies were buffer-exchanged into PBS using Zeba desalting columns (Thermo Fisher) prior to modification. Then, 200 μg of antibodies were reacted with the respective amine-reactive TCO or dye in 500 μL of PBS containing 10% DMF and 10% sodium bicarbonate for 3 h at room temperature. Modified antibodies were again purified and collected using Zeba spin desalting columns. Antibody and fluorophore concentrations were determined by absorption measurement using the NanoDrop.

Cell Culture.

MCF7 and MDA-MB-231 cell lines were maintained in DMEM media with 10% fetal bovine serum (FBS) and 1% Pen/Strep. MCF7 cell culture media was additionally supplemented with 1% L-glutamine, 1% nonessential amino acids (NEAA), 1 mM sodium pyruvate, and 10 μg/mL insulin. SK-BR-3 cells were grown in McCoy's 5A media with 10% FBS, 1% Pen/Strep, and 1% L-glutamine. MCF10A cells were cultured in DMEM/F12 media containing 5% horse serum, 1% Pen/Strep, 20 ng/mL EGF, 0.5 μg/mL hydrocortisone, 100 ng/mL cholera toxin, and 10 μg/mL insulin. The cells were seeded in T-75 flasks, incubated at 37 °C with 5% CO_2, and subcultured upon reaching ~80% confluency. Prior to imaging, the cells were grown in glass chamber wells (Lab Tek; Thermo Fisher) for 2–3 days. For surface markers, the cells were incubated with modified antibodies (10 μg/mL) in 200 μL of PBS+ for 30 min at room temperature. For quantum dots, the cells were first incubated with TCO-anti-EpCAM and subsequently stained with 200 nM tetrazine-Qdot 585 for 30 min at room temperature. The cells were washed three times with PBS+ after each incubation. For intracellular markers, the cells were fixed using a 1:1 mixture of PBS and Fix Buffer 1 (BD Biosciences) at room temperature for 15 min. The cells were then permeabilized by washing three times with Perm/Wash buffer containing 1% BSA (PW+, BD Biosciences). Antibody staining was then performed as described above, but using PW + as the buffer, and the cells were washed with PBS+ prior to imaging.

Imaging and Data Analysis.

Fluorescence intensity was measured using a multichannel upright laser scanning confocal microscope (FV1000; Olympus) with a 60× water immersion objective lens and a 20 MHz Fianium laser. Samples were excited at 534 ± 20 nm wavelength and the emission signal was collected in a 560–660 nm wavelength window. The acquisition speed was set to 20.0 μs/pixel and the pinhole size was 2.0 μm. A total of four frames were captured for each confocal image with Fluoview software (Ver. 02.01; Olympus). Brightness was set via the intensity threshold for optimal visualization, and the mean intensity was analyzed using Fiji

ImageJ software (Version 2.0.0; Bethesda). Lifetime information was acquired by an A320 FastFLIM FLIMbox (ISS) and directly transformed onto the phasor plot using SimFCS-64 software developed by the Laboratory for Fluorescence Dynamics at the University of California, Irvine. A total of 50 frames were collected for each image for FLIM analysis. Rhodamine 110, with a known lifetime of 4 ns, was employed for lifetime calibration. Photon cutoff was set to >1 photon per pixel when processing FLIM data using SimFCS-64 software to reduce the background signal. Cursors with different colors were selected for defining phasor locations of pure species. The fractional contribution of each component was calculated using SimFCS-64 software. Briefly, the relative contribution of each probe was determined using the linear combination rule. Since lifetime information for each pixel was mapped onto the phasor by Fourier transformation, the vector addition property of Fourier space was valid for the phasor space. Specifically, the cloud of pixels containing two probe species must lie on the line connecting the phasor locations of the two pure probe species. For three probe species within a pixel, the phasor location fell inside the triangle formed by the vertices of the three pure probe species. The fractional contribution of each individual component in the mixture was therefore inversely proportional to the distance to each pure probe species location.[41–44] The sum of fractional contributions for all components must be equal to 1 within each pixel. Fractional contributions for an entire image were calculated by SimFCS-64 software and averaged over multiple images to determine the mean fractional contribution. The intensity for each biomarker probe was determined for individual images by multiplying the fractional contribution and total intensity. The mean intensity was then calculated for all pixels exhibiting detectable fluorescence intensity across multiple images. Zerointensity pixels were excluded using the threshold function in Fiji.

Supplementary Material

Refer to Web version on PubMed Central for supplementary material.

ACKNOWLEDGMENTS

The authors would like to thank Dr. Hongtao Chen for assistance with imaging and analysis. This work was supported by the National Institutes of Health (NIH) National Cancer Institute (NCI) under Award Numbers R21CA206953 and P30CA062203, as well as the American Cancer Society under Institutional Research Grant 129801-IRG-16-187-13-IRG. H.P. was funded by the University of California, Irvine's Medical Scientist Training Program of the National Institutes of Health under award number T32GM008620. The content is solely the responsibility of the authors and does not necessarily represent the official views of the National Institutes of Health and American Cancer Society.

REFERENCES

(1). Stadler C; Rexhepaj E; Singan VR; Murphy RF; Pepperkok R; Uhlen M; Simpson JC; Lundberg E Nat. Methods 2013, 10, 315–323. [PubMed: 23435261]

(2). Croce AC; Bottiroli G Eur. J. Histochem. 2014, 58, 2461. [PubMed: 25578980]

(3). Surre J; Saint-Ruf C; Collin V; Orenga S; Ramjeet M; Matic I Sci. Rep. 2018, 8, No. 12088. [PubMed: 30108248]

(4). Walsh AJ; Mueller KP; Tweed K; Jones I; Walsh CM; Piscopo NJ; Niemi NM; Pagliarini DJ; Saha K; Skala MC Nat. Biomed. Eng. 2021, 5, 77–88. [PubMed: 32719514]

(5). Stringari C; Cinquin A; Cinquin O; Digman MA; Donovan PJ; Gratton E Proc. Natl. Acad. Sci. U.S.A. 2011, 108, 13582–13587. [PubMed: 21808026]

(6). Wright BK; Andrews LM; Markham J; Jones MR; Stringari C; Digman MA; Gratton E Biophys. J. 2012, 103, L7–L9. [PubMed: 22828352]

(7). Datta R; Alfonso-Garcia A; Cinco R; Gratton E Sci. Rep. 2015, 5, No. 9848. [PubMed: 25993434]

(8). Resch-Genger U; Grabolle M; Cavaliere-Jaricot S; Nitschke R; Nann T Nat. Methods 2008, 5, 763–775. [PubMed: 18756197]

(9). Zrazhevskiy P; Gao X Nat. Commun. 2013, 4, No. 1619. [PubMed: 23511483]

(10). Colyer RA; Lee C; Gratton E Microsc. Res. Tech. 2008, 71, 201–213. [PubMed: 18008362]

(11). Stringari C; Edwards RA; Pate KT; Waterman ML; Donovan PJ; Gratton E Sci. Rep. 2012, 2, No. 568. [PubMed: 22891156]

(12). Stringari C; Sierra R; Donovan PJ; Gratton EJ Biomed. Opt. 2012, 17, No. 046012.

(13). Chakraborty S; Nian FS; Tsai JW; Karmenyan A; Chiou A Sci. Rep. 2016, 6, No. 19145. [PubMed: 26758390]

(14). Lee DH; Li X; Ma N; Digman MA; Lee AP Lab Chip 2018, 18, 1349–1358. [PubMed: 29638231]

(15). Dong Y; Digman MA; Brewer GJ Geroscience 2019, 41, 51–67. [PubMed: 30729413]

(16). Alfonso-García A; Smith TD; Datta R; Luu TU; Gratton E; Potma EO; Liu WF J. Biomed. Opt. 2016, 21, 046005. [PubMed: 27086689]

(17). Plotegher N; Stringari C; Jahid S; Veronesi M; Girotto S; Gratton E; Bubacco L FASEB J. 2015, 29, 2484–2494. [PubMed: 25713058]

(18). Trinh AL; Chen H; Chen Y; Hu Y; Li Z; Siegel ER; Linskey ME; Wang PH; Digman MA; Zhou YH Cancers 2017, 9, 168. [PubMed: 29211022]

(19). Jeong S; Greenfield DA; Hermsmeier M; Yamamoto A; Chen X; Chan KF; Evans CL Sci. Rep. 2020, 10, No. 5360. [PubMed: 32210332]

(20). Osseiran S; Roider EM; Wang H; Suita Y; Murphy M; Fisher DE; Evans CL J. Biomed. Opt. 2017, 22, 1–10.

(21). Ranjit S; Datta R; Dvornikov A; Gratton EJ Phys. Chem. A 2019, 123, 9865–9873.

(22). Hinde E; Digman MA; Welch C; Hahn KM; Gratton E Microsc. Res. Tech. 2012, 75, 271–281. [PubMed: 21858900]

(23). Hinde E; Digman MA; Hahn KM; Gratton E Proc. Natl. Acad. Sci. U.S.A. 2013, 110, 135–140. [PubMed: 23248275]

(24). Llères D; Bailly AP; Perrin A; Norman DG; Xirodimas DP; Feil R Cell Rep. 2017, 18, 1791–1803. [PubMed: 28199849]

(25). Lou J; Scipioni L; Wright BK; Bartolec TK; Zhang J; Masamsetti VP; Gaus K; Gratton E; Cesare AJ; Hinde E Proc. Natl. Acad. Sci. U.S.A. 2019, 116, 7323–7332. [PubMed: 30918123]

(26). Akers W; Lesage F; Holten D; Achilefu S Mol. Imaging 2007, 6, 237–246. [PubMed: 17711779]

(27). Ardeshirpour Y; Chernomordik V; Zielinski R; Capala J; Griffiths G; Vasalatiy O; Smirnov AV; Knutson JR; Lyakhov I; Achilefu S; Gandjbakhche A; Hassan M PLoS One 2012, 7, No. e31881. [PubMed: 22384092]

(28). Okkelman IA; Dmitriev RI; Foley T; Papkovsky DB PLoS One 2016, 11, No. e0167385. [PubMed: 27973570]

(29). Jena S; Damayanti NP; Tan J; Pratt ED; Irudayaraj JMK; Parker LL Chem. Commun. 2020, 56, 13409–13412.

(30). Kashirina AS; Lopez-Duarte I; Kubankova M; Gulin AA; Dudenkova VV; Rodimova SA; Torgomyan HG; Zagaynova EV; Meleshina AV; Kuimova MK Sci. Rep. 2020, 10, No. 14063. [PubMed: 32820221]

(31). Orte A; Alvarez-Pez JM; Ruedas-Rama MJ ACS Nano 2013, 7, 6387–6395. [PubMed: 23808971]

(32). Hoffmann K; Behnke T; Drescher D; Kneipp J; Resch-Genger U ACS Nano 2013, 7, 6674–6684. [PubMed: 23837453]

(33). Battisti A; Digman MA; Gratton E; Storti B; Beltram F; Bizzarri R Chem. Commun. 2012, 48, 5127–5129.

(34). Maus M; Cotlet M; Hofkens J; Gensch T; De Schryver FC; Schaffer J; Seidel CA Anal. Chem. 2001, 73, 2078–2086. [PubMed: 11354494]

(35). Pelet S; Previte MJ; Laiho LH; So PT Biophys. J. 2004, 87, 2807–2817. [PubMed: 15454472]

(36). Grabolle M; Kapusta P; Nann T; Shu X; Ziegler J; Resch-Genger U Anal. Chem. 2009, 81, 7807–7813. [PubMed: 19705851]

(37). de Grauw CJ; Gerritsen HC Appl. Spectrosc. 2001, 55, 670–678.

(38). Soloviev VY; Tahir KB; McGinty J; Elson DS; Neil MA; French PM; Arridge SR Appl. Opt. 2007, 46, 7384–7391. [PubMed: 17952172]

(39). Algar WR; Wegner D; Huston AL; Blanco-Canosa JB; Stewart MH; Armstrong A; Dawson PE; Hildebrandt N; Medintz IL J. Am. Chem. Soc. 2012, 134, 1876–1891. [PubMed: 22220737]

(40). Niehörster T; Loschberger A; Gregor I; Kramer B; Rahn HJ; Patting M; Koberling F; Enderlein J; Sauer M Nat. Methods 2016, 13, 257–262. [PubMed: 26808668]

(41). Digman MA; Caiolfa VR; Zamai M; Gratton E Biophys. J. 2008, 94, L14–L16. [PubMed: 17981902]

(42). Ranjit S; Malacrida L; Jameson DM; Gratton E Nat. Protoc. 2018, 13, 1979–2004. [PubMed: 30190551]

(43). Torrado B; Malacrida L; Ranjit S Sensors 2022, 22, No. 999. [PubMed: 35161742]

(44). Vallmitjana A; Dvornikov A; Torrado B; Jameson DM; Ranjit S; Gratton E Methods Appl. Fluoresc. 2020, 8, No. 035001. [PubMed: 32235070]

(45). Vallmitjana A; Torrado B; Dvornikov A; Ranjit S; Gratton EJ Phys. Chem. B 2020, 124, 10126–10137.

(46). Cutrale F; Trivedi V; Trinh LA; Chiu CL; Choi JM; Artiga MS; Fraser SE Nat Methods 2017, 14, 149–152. [PubMed: 28068315]

(47). Scipioni L; Rossetta A; Tedeschi G; Gratton E Nat Methods 2021, 18, 542–550. [PubMed: 33859440]

(48). Vu T; Vallmitjana A; Gu J; La K; Xu Q; Flores J; Zimak J; Shiu J; Hosohama L; Wu J; Douglas C; Waterman ML; Ganesan A; Hedde PN; Gratton E; Zhao W Nat. Commun. 2022, 13, No. 169. [PubMed: 35013281]

(49). Zrazhevskiy P; True LD; Gao X Nat. Protoc. 2013, 8, 1852–1869. [PubMed: 24008381]

(50). Goltsev Y; Samusik N; Kennedy-Darling J; Bhate S; Hale M; Vazquez G; Black S; Nolan GP Cell 2018, 174, 968–981.e15. [PubMed: 30078711]

(51). Schürch CM; Bhate SS; Barlow GL; Phillips DJ; Noti L; Zlobec I; Chu P; Black S; Demeter J; McIlwain DR; Kinoshita S; Samusik N; Goltsev Y; Nolan GP. Cell 2020, 182, 1341–1359.e19. [PubMed: 32763154]

(52). Haun JB; Castro CM; Wang R; Peterson VM; Marinelli BS; Lee H; Weissleder R Sci. Transl. Med. 2011, 3, No. 71ra16.

(53). Martowicz A; Spizzo G; Gastl G; Untergasser G BMC Cancer 2012, 12, 501. [PubMed: 23110550]

(54). Soysal SD; Muenst S; Barbie T; Fleming T; Gao F; Spizzo G; Oertli D; Viehl CT; Obermann EC; Gillanders WE Br. J. Cancer 2013, 108, 1480–1487. [PubMed: 23519058]

(55). Haun JB; Devaraj NK; Hilderbrand SA; Lee H; Weissleder R Nat. Nanotechnol. 2010, 5, 660–665. [PubMed: 20676091]

(56). Haun JB; Devaraj NK; Marinelli BS; Lee H; Weissleder R ACS Nano 2011, 5, 3204–3213. [PubMed: 21351804]

(57). Rahim MK; Kota R; Haun JB Bioconjugate Chem. 2015, 26, 352–360.

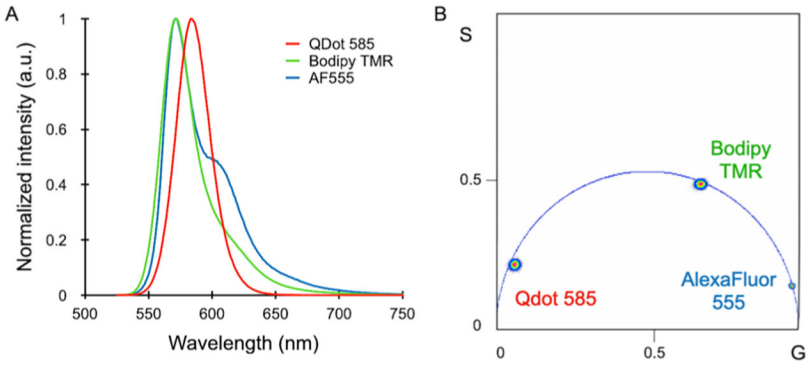

Figure 1.

Properties of the lifetime probe panel. (A) Emission spectrum and (B) phasor diagram locations for the Qdot 585, Bodipy TMR, and AF555 fluorescence lifetime probes. Lifetime measurements were obtained by the FLIM of probes in PBS buffer after conjugation to an antibody.

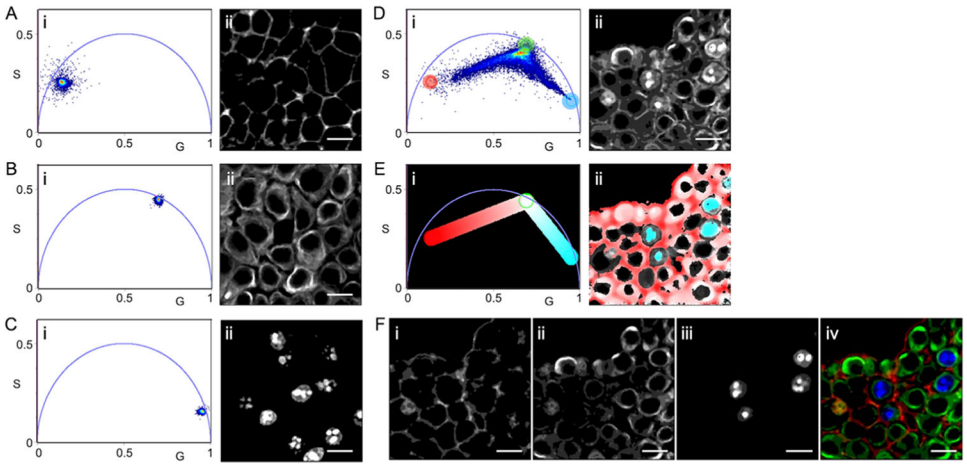

Figure 2.

Detection of spatially separated biomarkers on MCF7 cells. (A–C) Cells were labeled with (A) αEpCAM-Qdot 585, (B) αCK18-Bodipy TMR, (C) αKi67-AF555, or (D) the mixture of all three, and the results are shown for the (i) phasor diagram and (ii) total intensity image. Colored circles in the combined phasor in part (D(i)) correspond to the pure probe species from parts (A–C(i)). (E) Results from part (D) were painted with a color gradient to convey relative probe contributions. (F) Probe contributions were fully resolved and pure species images were generated for (i) αEpCAM-Qdot 585, (ii) αCK18-Bodipy TMR, and (iii) αKi67-AF555. (F(iv)) Pseudocolored overlay showing EpCAM in red, CK18 in green, and Ki67 in blue. Scale bars represent 20 μm.

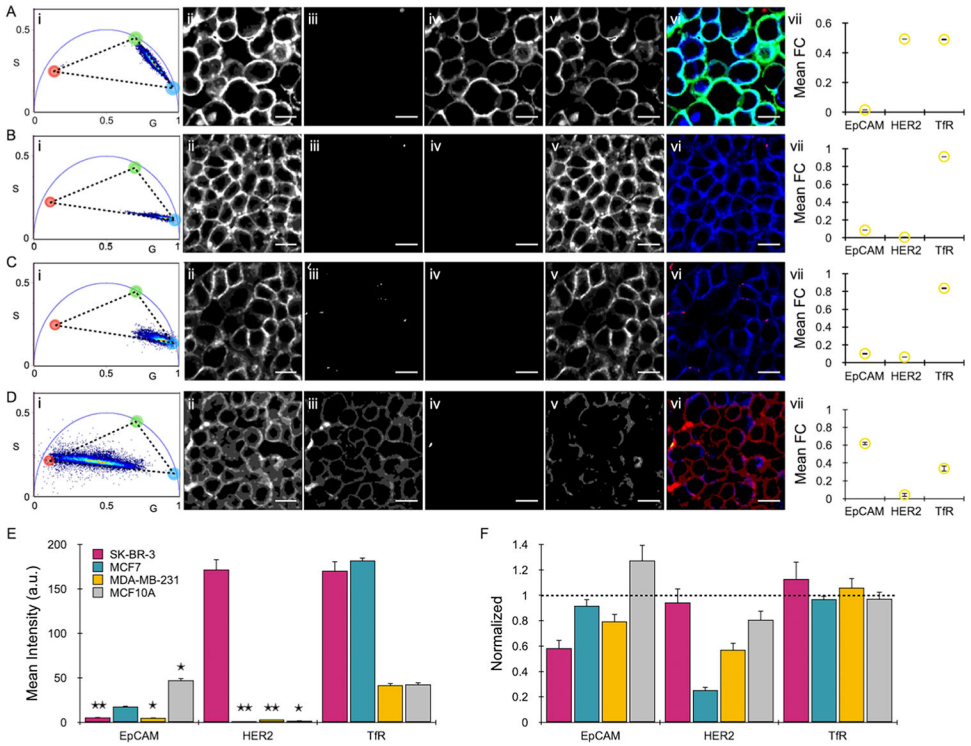

Figure 3.

Detection of spatially colocalized biomarkers. Breast cancer cell lines (A) SK-BR-3, (B) MCF7, (C) MDA-MB-231, and (D) MCF10A were labeled with a mixture of αEpCAM-Qdot 585, αHER2-Bodipy TMR, and αTfR-AF555. Results are shown for a representative (i) phasor plot; (ii) total intensity image; resolved individual intensity images for (iii) EpCAM, (iv) HER2, and (v) TfR; and (vi) pseudocolored overlay image (red EpCAM, green HER2, blue TfR). Additionally, multiple images were analyzed to determine (vii) the mean fractional contribution (FC) of each probe. (E) Mean intensity for each biomarker probe was calculated by multiplying probe contribution by total mean intensity. (F) Results in part (E) were normalized by the mean intensity of single-stain images for the same biomarker–probe combination and cell line, shown in Figure S4 in the Supporting Information. Error bars represent the standard error from at least three independent experiments. Stars indicate $p < 0.05$ and double stars indicate $p < 0.01$ relative to the single-stain mean intensity for the same biomarker probe and cell line (see Figure S4 in the Supporting Information). Scale bars represent 20 μm.

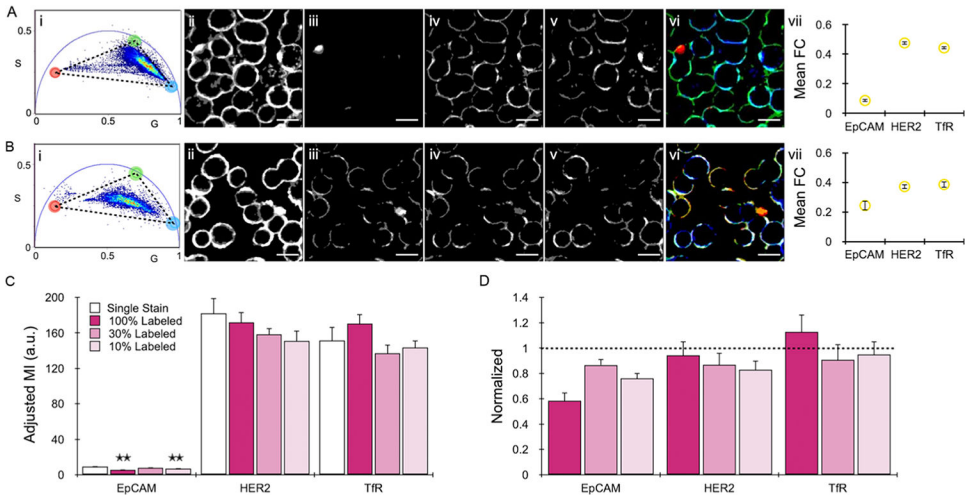

Figure 4.

Intensity matching for SK-BR-3 cells. Signal intensities for αHER2-Bodipy TMR and αTfR-AF555 probes were lowered by the addition of the unlabeled antibody at labeled/unlabeled ratios of (A) 30:70 and (B) 10:90. αEpCAM-Qdot 585 was used without dilution. The results are shown for representative (i) phasor plot; (ii) total intensity image; resolved individual intensity images for (iii) EpCAM, (iv) HER2, and (v) TfR; and (vi) pseudocolored overlay image (red EpCAM, green HER2, blue TfR), as well as (vii) mean fractional contribution (FC) of each probe from multiple images. (C) Mean intensity for each probe, adjusted for dilution using calibrations given in Figure S5 in the Supporting Information. Nondiluted single stain (from Figure S4 in the Supporting Information) and resolved triple stain results (from Figure 3) are shown for comparison. (D) Adjusted mean intensity normalized by the nondiluted single stain. Error bars represent the standard error from at least three independent experiments. Stars indicate $p < 0.05$ and double stars indicate $p < 0.01$ relative to the mean intensity single stain for the same biomarker probe. Scale bars represent 20 μm.

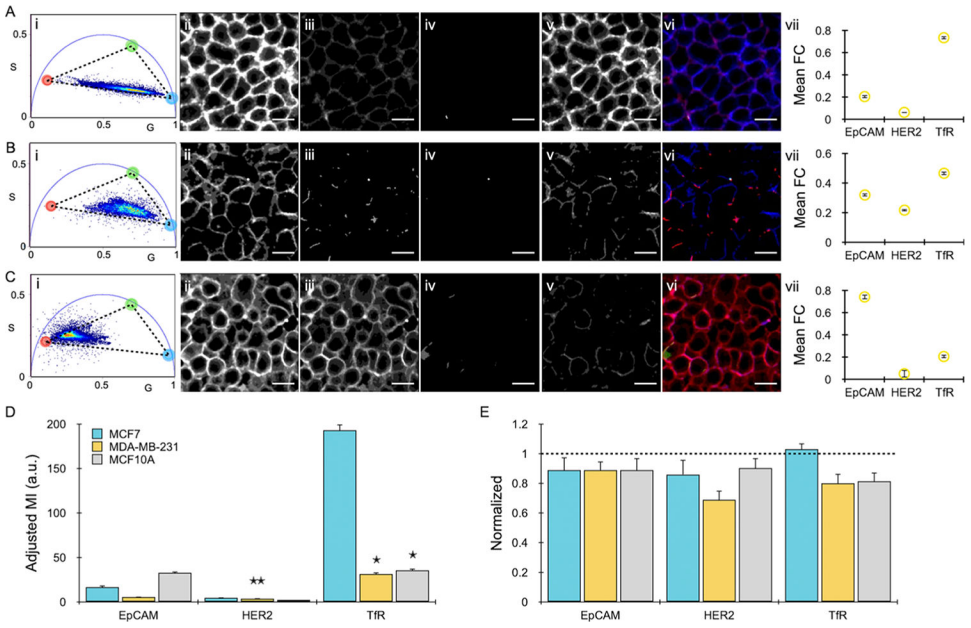

Figure 5.

Intensity matching for other cell lines. (A) MCF7, (B) MDA-MB-231, and (C) MCF10A cell lines were labeled with αEpCAM-Qdot 585, αHER2-Bodipy TMR, and αTfR-AF555 (30:70 ratio TfR-labeled/unlabeled). The results are shown for representative (i) phasor plot; (ii) total intensity image; resolved individual intensity images for (iii) EpCAM, (iv) HER2, and (v) TfR; and (vi) pseudocolored overlay image (red EpCAM, green HER2, blue TfR), as well as (vii) mean fractional contribution (FC) of each probe from multiple images. (D) Mean intensity, adjusted for dilution using calibrations given in Figure S6 in the Supporting Information. (E) Adjusted mean intensity normalized by nondiluted single-stain images for the same biomarker–probe combination and cell line, shown in Figure S4 in the Supporting Information. Error bars represent the standard error from at least three independent experiments. Stars indicate $p < 0.05$ and double stars indicate $p < 0.01$ relative to the nondiluted single-stain mean intensity for the same biomarker–probe and cell line (see Figure S4 in theSupporting Information). Scale bars represent 20 μm.

Table 1.

Optimal Labeling Conditions and FLIM/Phasor Reporting Accuracies for Each Biomarker and Cell Line[a]

	EpCAM			HER2			TfR		
cell line	**best condition**	**accuracy (%)**	**fig.**	**best condition**	**accuracy (%)**	**fig.**	**best condition**	**accuracy (%)**	**fig.**
SKBR3	HER2&TfR dilution (30%)	86.7 ± 4.7	Figure 4A	no dilution	94.4 ± 10.9	Figure 3A	no dilution	112.8 ± 13.4	Figure 3A
MCF7	TfR dilution (30%)	88.9 ± 8.7	Figure 5A	TfR dilution (30%)	85.9 ± 9.9	Figure 5A	no dilution	96.9 ± 2.6	Figure 3B
MDA-MB-231	TfR dilution (30%)	89.0 ± 5.6	Figure 5B	TfR dilution (30%)	68.9 ± 6.2	Figure 5B	no dilution	105.9 ± 7.5	Figure 3C
MCF10A	TfR dilution (30%)	88.9 ± 8.1	Figure 5C	TfR dilution (30%)	90.3 ± 6.7	Figure 5C	no dilution	97.1 ± 5.5	Figure 3D

[a]Accuracy refers to the comparison of mean fluorescence intensity to the corresponding single-probe case, reported as percentage. All conditions were statistically similar to the single-probe case.